Correlation of GEO Communications Satellite Anomalies and Space Weather Phenomena: Improved Satellite Performance and Risk Mitigation

Whitney Q. Lohmeyer[1] and Kerri Cahoy[2]
MIT, Cambridge, MA, 02139

and

Daniel N. Baker[3]
University of Colorado, Boulder, CO, 80309-0390

We correlate on-orbit component telemetry data from seven Inmarsat geostationary communications satellites from 1996 to 2012 with historical space weather information. We specifically utilize data from the Geostationary Operational Environment Satellites (GOES), the Advanced Composition Explorer (ACE) Satellite, the Royal Observatory of Belgium's Solar Influences Data Analysis Center (SIDC), and the Kyoto Geomagnetic Equatorial Disturbance Storm Time (Dst) Index data service. In our analysis, we compare the Inmarsat solid-state power amplifier (SSPA) currents to energetic particle fluxes and space weather indices such as Dst, Kp (an index that describes disturbances in horizontal component of the Earth's magnetic field), and solar flares. These space weather indices capture the severity of solar storms that can send energetic particles streaming towards Earth and magnetic storms that can impact the performance of GEO communication satellites. We find that seventeen out of twenty-six SSPA anomalies occurred within two weeks of prior severe space weather events. Two anomalies occurred during geomagnetic events, one occurred during a severe radiation event caused by solar energetic protons, and fifteen occurred within two weeks of severe radiation events caused by relativistic electrons. There was no apparent correlation between spacecraft eclipse periods and anomaly occurrence. Although the year with the most anomalies coincided with a sunspot cycle minimum, there were additional fleet transition factors that prevent a clear conclusion about this aspect. Additional findings include an interesting direct relationship between the GOES 2 MeV electron flux and SSPA current prior to an anomaly. Anomalies with on-board components such as SSPAs are expected and are managed by all satellite operators. An anomaly rate is factored into the design of geostationary satellites and is typically mitigated through the use of on-board unit redundancy and configuration options. The examples given have been handled without impacting the performance of any satellite. The current SSPA anomaly rate is significantly lower than that modeled as part of the design reliability analysis, hence both performance and lifetime have not been impacted adversely.

I. Introduction

Inmarsat has been operating its own geostationary (GEO) communications satellite fleet since 1990. The company maintains an archive of component telemetry and housekeeping data for the purpose of monitoring the satellites' primary system functions. Satellite performance and component anomalies are detected with thresholds used to filter the real-time data transmitted from orbit.

[1]Graduate Student, MIT AeroAstro, 77 Massachusetts Avenue, Cambridge, MA 02139, AIAA Member.
[2]Assistant Professor, MIT AeroAstro, 77 Massachusetts Avenue, Cambridge, MA 02139, AIAA Member.
[3]Professor, LASP/CU-Boulder, 3665 Discovery Drive, Boulder, CO 80303-7820, and AIAA Member.

However, outside of fleet maintenance, scientific analyses to understand the physical causes of historic component anomalies are generally limited. In collaboration with Inmarsat, in this work, we pursue an improved level of understanding the Inmarsat housekeeping data, using a subset of the archive to enable an investigation into how space weather affects satellite performance. The relationship between space weather and performance is an area of particular interest for both Inmarsat and the space weather community.

Space weather affects the performance and overall lifetime of GEO satellites. However, much work remains to be done in order to achieve an in-depth understanding of the specific types of space weather events that significantly impact component health, and the necessary methods for mitigating component failures. Understanding the causal relationship between space weather and component health is important because this knowledge will help improve the robustness of satellite hardware and thus improve the services that satellite operators provide to their customers.

We compare Inmarsat solid-state power amplifier (SSPA) currents and solar panel power to energetic particle fluxes, Kp, and the Disturbance Storm Time (Dst) Index. These space weather indices reflect the severity of solar storms that can send energetic particles streaming towards Earth and the resulting geomagnetic storms that affect the morphology of the magnetosphere at the altitude of GEO communication satellites. We find correlations between space weather events and satellite component anomalies as a function of time, age of the spacecraft, and satellite location.

In Section II, we describe how different types and energy levels of solar particles affect spacecraft systems. Section III details the geomagnetic indices and scheme for classification of severe space weather events used in this work. We present both the spacecraft and space weather data used in Section IV, discuss results in Section V, and summarize our results and identify our path forward in Section VI.

II. Space Weather: Particles, Energy Levels, and Their Effects on Spacecraft Systems

A. Background

The space radiation environment is an important aspect of satellite design that should be accounted for to meet the satellite's performance and lifetime requirements. Advances in technology have led to a reduction in the size of satellite components – on the micro and nano scales –, which has increased their susceptibility to the effects of space weather[1,2,3]. Electrical upsets, interference, and solar array degradation are just a few of the known effects. As a result of space weather, satellite operators are occasionally forced to manage reduced performance and capacity or fully decommission satellites, amounting to social and economic losses equivalent to several tens of millions of dollars per year[4].

A constant flow of radiation, plasma, and energetic particles originates from the Sun in the form of solar wind. This wind flows through the solar system and interacts with planets and their magnetic fields. While the solar wind in its nominal state can sometimes contribute to anomalies, the more serious threat of space weather comes from violent solar eruptions known as coronal mass ejections (CMEs) and solar flares. These bursts of energy and mass originate at sunspots, well-defined areas of cooler temperatures on the Sun's surface that appear as regions of dark spots. At these surface spots, strong magnetic field fluctuations can cause the energy and matter to become unstable and launch into space. CMEs and solar flares send high-speed solar wind, carrying charged particles and intense magnetic fields at speeds of up to 3000 km/s, into the Earth's magnetosphere, ionosphere, and thermosphere. Solar flare X-rays can reach Earth's surface in eight minutes (i.e., at the speed of light), whereas solar energetic particles take closer to an hour. The highly energetic particles, ranging from ten to hundreds of MeV, deposit themselves into the surface and electronics of spacecraft, and are one of the most common causes of satellite anomalies[5].

During geomagnetic storms and solar proton events, charged particles are also capable of penetrating the surface of satellites and bombarding the spacecraft's electrical components, which can ultimately lead to an electrical breakdown. When considering geostationary satellite systems, the primary particles of interest are low-energy electrons, high-energy electrons and high-energy protons. These particles are notoriously considered the sources of surface charging, bulk dielectric charging, and single event upsets/solar array degradation, respectively.

The common metric used to assess the overall strength and variation of solar activity, such as solar flares and CMEs, is the sunspot number. The increase and decrease in sunspot number defines the solar maximum and solar minimum. At solar maximum there is an increased chance of solar flares and other solar disturbances, however even at solar minimum the Sun can produce damaging storms[6]. When the solar activity progresses between a high and low sunspot number, it defines the solar magnetic activity cycle, a period of approximately eleven years.

Figure **1** depicts the sunspot number, the smoothed sunspot number, and all 26 SSPA anomalies between the years 1996 and 2012. This time period encompasses Solar Cycle 23 (May 1996 – Dec. 2008) and Solar Cycle 24 (Jan. 2009 – present). The solar maximum for Cycle 23 occurred approximately between 1998-2002, and the solar minimum occurred approximately between 2006 and 2009. The solar maximum has yet to occur for Cycle 24. The data for this plot are from the Royal Observatory of Belgium's Solar Influences Data Analysis Center (SIDC)[7].

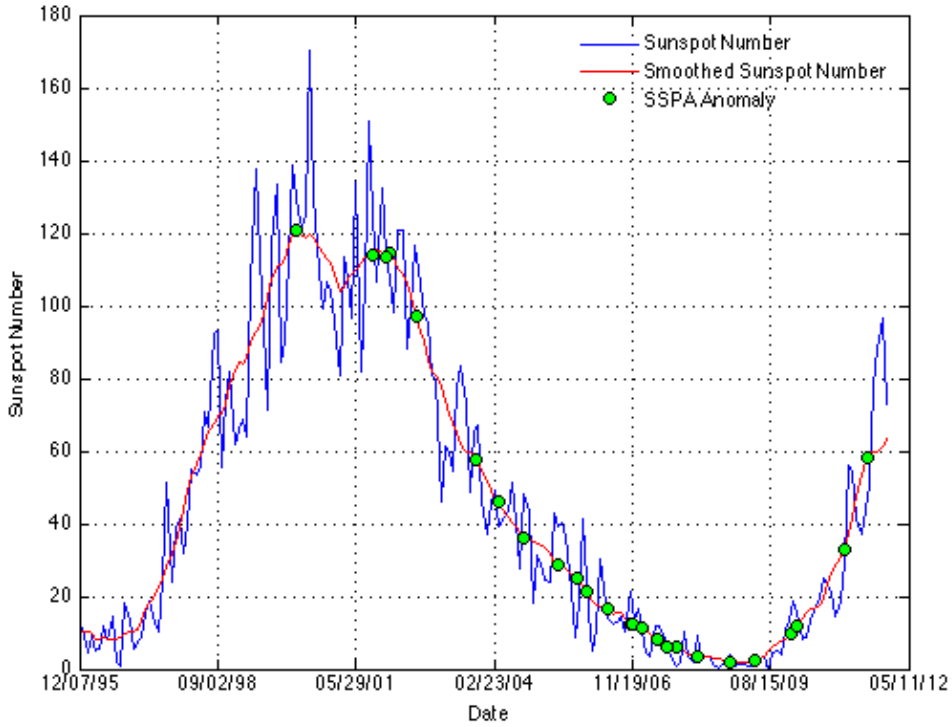

Figure 1: Solar Cycle 23 and Solar Cycle 24 Sunspot Number, Smoothed Sunspot Number, and Inmarsat SSPA Anomalies

In Figure **1** there are clearly more anomalies that occur during solar minimum than at solar maximum. However, a conclusive correlation between anomalies and solar cycle cannot be unambiguously stated, because the twenty-six anomalies plotted in Figure 1 are from two separate satellite fleets. One of the fleets launched approximately ten years prior to the second, thus the number of satellites incrementally increased from zero to seven between 1996-1998 as well as in 2005-2008.

B. Low Energy Electrons

The expulsion of low-energy electrons, ranging in energy between approximately 10-100 keV, is a hazardous result of magnetospheric substorms. When these low-energy electrons interact with GEO satellites, they deposit their charge onto the surface of the satellite, but they are typically too low in energy to penetrate the structure's surface[1].

The accumulation of charged particles on insulating surfaces can lead to a buildup of charge, and ultimately cause arcing or a breakdown discharge. However, instead of developing in the dielectric materials of the spacecraft, the charge buildup occurs on its surface. If inadequate electrical connections exist between the solar arrays and surface materials, then differential charging on the surface can cause lightning-like breakdown discharges between the materials. Furthermore, differential charging at GEO is directly related to local time, showing a distinct tendency for surface charging from a local time of midnight until dawn[8]

C. High-Energy Electrons

Relativistic electrons (with energies greater than ~300 keV), are commonly referred to as high-energy electrons and cause deep dielectric or bulk charging. Bulk charging generally occurs hours to days after

large magnetic storms and results from high-energy electrons that penetrate the surface-shielding material of a satellite. Once the electrons penetrate the surface, they can deposit into the spacecraft's thick dielectrics, including cables, conductors and circuit boards. Interaction with high-energy electrons can significantly change the electrical properties of dielectric materials. If bulk charging occurs at a rate greater than the existing charge can escape from the dielectric, then a breakdown can possibly occur. A breakdown generates a fast pulse, 100 nanoseconds or less, on connected devices and discharges energy into sensitive electronic circuits.

An electrical discharge occurs when the field between two materials accumulates and exceeds a critical threshold. Often, discharge stems from sharp flux changes, or when surfaces have different conductivities[3]. Discharges can introduce noise into the system, cause interference, cause serious component damage, cause a bit flip, or completely interrupt spacecraft operation[9]. At GEO, the intensity of high-energy electrons can penetrate spacecraft shielding, cause operational anomalies, and even lead to satellite failures[10].

D. High-Energy Protons

High-energy protons, or solar energetic particles (SEPs), have energies of approximately 30 MeV or greater, resulting from powerful solar disturbances. They have been shown to cause single event upsets (SEU) and solar array degradation. The term SEU is commonly used within the satellite industry to indicate when high energy-particles cause electrical interference such as a 'bit flip', physical damage, and even component failure[10]. SEUs can occur at any point throughout the eleven-year solar cycle, but are found to mostly occur near solar minimum, between the second and ninth year of the typical 11-year solar cycle[2]. The causal relationship between high-energy protons, SEUs and solar array degradation is of particular interest to the communications satellite industry as these interactions are not well understood.

III. Geomagnetic Indices and Definition of Severe Space Weather Events

A. Geomagnetic Indices

The strength of the Earth's magnetic field can be measured using a number of different indices. Two of the most commonly used indices used for describing geomagnetic storms are Kp and Dst.

Kp is the general planetary index used for qualitatively characterizing the high latitude geomagnetic environment. This parameter is determined from a network of ground-based magnetometer measurements, and is the weighted average of the maximum value of the horizontal component of the magnetic field during a three-hour period[11,12]. The Kp scale spans from zero to nine, where nine describes the highest level of severity for geomagnetic storms.

The second metric for geomagnetic activity is Dst, which is a quantitative measure for the severity of geomagnetic storms. Dst is the mean of the horizontal component of the Earth's magnetic field measured at four ground-based observatories located in Hawaii, Puerto Rico, South Africa and Japan. For "typical" magnetic storms Dst undergoes the following phases[13]:

1. Nominal Phase: Before a magnetic storm, Dst measures approximately zero; this is the condition for a quiet day, or a period of low geomagnetic activity.
2. Main Phase Stage 1: As the magnetic storm begins, the Dst will initially increase due to the compression of the magnetosphere that occurs from interplanetary shocks in the initial phase of the storm.
3. Main Phase Stage 2: Dst drastically decreases as the intensity of trapped particles heightens.
4. Recovery Phase: After the strength of the magnetic storm peaks (occasionally on the order of -400 nT), Dst will begin to increase back toward its baseline value.

During a magnetic storm Dst becomes negative, because as the intensity of the storm increases as the number of electrons and low-energy ions located in the magnetosphere increases. These energetic particles comprise the "ring current." As ring current increases during magnetic storms, Dst decreases because it is inversely proportional to the energy of the ring current[6]. However, once the interplanetary magnetic field returns toward more nominal values, the ring current returns to a quiet level and Dst increases. At lower latitudes, the magnetic strength on the surface of the Earth is proportional to the energy of the ring current[13].

B. Severe Space Weather Events

While there are numerous databases of recorded space weather metrics (GOES, Kyoto, and ACE) a common list of historical severe space weather events does not exist. This is partly due to the multitude of variations one discovers when attempting to define the term "severe space weather event." For this work, we have developed a definition for "severe space weather event" based on four categories: (i) geomagnetic storms, (ii) energetic protons radiation storm, (iii) relativistic electrons radiation storm, and (iv) solar flare X-rays. These metrics are based on NOAA Space Weather Prediction Center's (SWPC) Space Weather Alerts and criteria used in recent studies throughout the space weather community[14].

A severe (i) geomagnetic storm occurs when Dst is less than -200 nT. We tabulated when Dst was less than -200 nT using the Kyoto Dst database. A severe radiation storm occurs when the 10 MeV proton flux exceeds 10,000 proton flux units (pfu, particles/sr·cm^2·s), which is S4 on the NOAA Severe Weather Scale, as well as when the 2 MeV electron flux is greater than 10,000 pfu. NOAA sends space weather alerts when the 2 MeV electron flux is greater than 1,000 pfu, however in this work, we have defined a severe relativistic electron radiation event as that in which the 2 MeV electron flux exceeds 10,000 pfu to more clearly distinguish between the higher flux events. Severe radiation storms were broken into two categories: (ii) solar energetic particles (SEPs), and (iii) relativistic electrons, because solar energetic particles vary independently of relativistic electrons. Both types of severe radiation storms were determined from GOES data. SEPs arise due to strong flares, CMEs, and interplanetary shock waves, which can be immediate effects of solar storms. Relativistic electrons tend to occur in response to high solar wind speeds once the CMEs reach Earth or from other high-speed solar wind streams, which are essentially independent of CMEs and interplanetary shockwaves. Lastly, a (iv) severe solar storm event occurs when solar flares exceed the X10 classification. This is known as an R4 severe storm on the NOAA Severe Weather Scale[14].

Table 1: Definition of Severe Space Weather Events used in this work.

Storm Type	Condition	Data Source
Geomagnetic Storm	Dst < -200 nT	Kyoto
Radiation Storm – SEP	10 MeV Proton Flux > 10,000 pfu	GOES
Radiation Storm – Relativistic Electrons	2 MeV Electron Flux > 10,000 pfu	GOES
Solar Storm	Solar Flares > X10	GOES

Figure **2** shows the four types of severe space weather events, defined in Table **1** between the years 1996 and 2012, and the twenty-six SSPA anomalies described in more detail in Section IV. Severe radiation events caused from relativistic electrons between 2000 and 2002 are not included in the plot below, because these values are not explicitly tabulated from the NOAA Space Weather Prediction Center. The shaded regions denote the annual eclipse seasons for the Inmarsat satellites, which are listed in Table **3**.

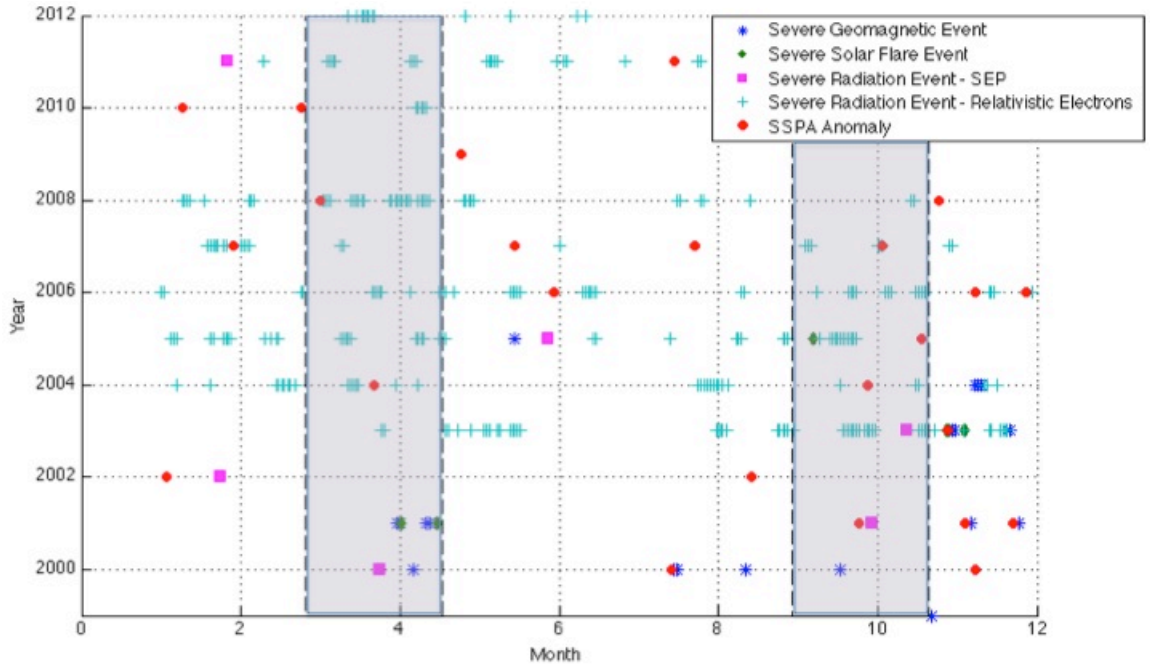

Figure 2: SSPA Anomalies and Severe Space Weather Events. SSPA anomalies are discussed in detail in Section IV; Severe Space Weather events are defined in Table 1 and listed in Appendix VII, except for the severe relativistic radiation event dates because of quantity.

Seventeen of the twenty-six SSPA anomalies occurred within two weeks of a severe space weather event. Of the seventeen SSPA anomalies that correlate with a severe space weather event, two occurred during a severe geomagnetic space weather event, one occurred during a severe radiation space weather event caused from SEPs, and fifteen of twenty-six SSPA anomalies occurred within two weeks of a severe radiation space weather event related to relativistic electrons. One of these fifteen SSPA anomalies also coincided with a severe geomagnetic space weather event.

There does not appear to be an increase of SSPA anomalies during eclipse seasons. A contributing factor to this may be the extensive safety measures Inmarsat takes to prepare its satellite fleets from performance degradation that may occur during an eclipse.

IV. Data Descriptions

In this work, four sets of spacecraft data are used, consisting of more than 500 MB of on-orbit component telemetry and anomaly data for Inmarsat's satellite fleet. We also use four archives of historical space weather data. Inmarsat's archive contains records of both nominal and anomalous component data from 1996 to 2012. For historical space weather information, we use data from the NOAA Geostationary Operational Environmental Satellites (GOES), the Geomagnetic Equatorial Dst Data Service in Kyoto, the Royal Observatory of Belgium's Solar Influences Data Analysis Center (SIDC) and the Advanced Composition Explorer (ACE) Satellite.

A. Inmarsat Historical Archives

This study focuses on seven of Inmarsat's geostationary communication satellites, which are located at different longitudes around the Earth's equator and which experience dynamic traffic loads. For these satellites, data on solid-state power amplifiers (SSPAs) and eclipse durations were analyzed, along with anomaly and SEU information for each satellite. Table 2 describes the collected Inmarsat satellite telemetry.

Table 2: Telemetry Descriptions

Telemetry Parameter	Description
SSPA Current	Solid-state power amplifier current
SSPA Temperature	Solid-state power amplifier temperature
Total Bus Power	Instantaneous power of the main power bus, power values are calculated from prime and redundant voltage and current sensors on the main bus
Solar Panel North/South Short Circuit Current	Output of the short-circuit cell current sensor located on the outboard panel of the north and south wing, used to determine when satellites are in eclipse
Solar Panel North/South Open Circuit Voltage	Output of the open-circuit cell voltage sensor located on the mid-board panel of the north and south wing

In this work, we tracked the start and end dates of eclipse season as well as the longest eclipse duration times for the four satellites with the highest traffic levels. Generally, geostationary satellites have a direct view of the sun and are able to primarily use energy right from the solar panels as a power source. However, during an eclipse, the Earth blocks sunlight from reaching the solar arrays and forces the satellite operators to monitor and control power management during the known eclipse seasons. The recorded eclipse dates are displayed in Table **3**. To simplify the table, instead of listing each range every year, we use the earliest eclipse start date since 1996, and the latest eclipse end date. Each year's eclipse duration is less than ten days long and falls within the range in Table **3**. The two eclipse seasons are from late February–mid-April and late August–late October; the longer eclipses last about 68 to 73 minutes.

Table 3: Summary of Eclipse Durations

Satellite	Spring Season Start	Spring Season End	Longest Eclipse Start	Longest Eclipse End	Fall Season Start	Fall Season End	Longest Eclipse Start	Longest Eclipse End
W	Feb. 25	April 15	March 16	March 24	Aug. 30	Oct. 19	Sept. 21	Sept. 26
X	Feb. 26	April 19	March 16	March 24	Aug. 30	Oct. 20	Sept. 21	Sept. 26
Y	Feb. 26	April 18	March 22	March 26	Aug. 30	Oct. 22	Sept. 25	Sept. 29
Z	Feb. 26	April 20	March 21	March 27	Aug. 30	Oct. 23	Sept. 21	Sept. 29

We also summarize general trends from the anomaly database, which includes anomalous activity, soft failures, hard failures, and SEUs. A soft failure is when a component's operating level drops or rises by a specified amount or threshold, but continues to operate at 25—50% of nominal operation. When a component's operating level drops to zero and becomes inoperable it is considered a hard failure. The term SEU is primarily used as a catchall term for an electrical anomaly. If a component experiences an unplanned power cycling, it is considered an SEU.

For the SEU analysis, we focus on the four satellites with the highest traffic. Of these satellites, two have advanced computing systems that consist of primary and secondary computers that are each susceptible to SEUs. The table below shows the distribution of SEUs over separate quarters of the year. However, when comparing the occurrence of SEUs with the different of eclipse seasons, no obvious correlation exists.

Table 4: Eclipse and SEU

Satellite	Nov. – Jan. Solstice	Feb. – April Equinox	May – July Solstice	Aug. – Oct. Equinox	Total SEUs
W	2	0	2	3	7
X	2	4	1	2	9
Y primary	2	3	3	8	16
Y secondary	7	11	14	13	45
Z primary	11	12	10	8	41
Z secondary	12	12	7	5	36

B. Geostationary Operational Environment Satellites (GOES) Data

To obtain dates for severe solar storm events (X-rays), radiation storm events (SEPs and relativistic electrons), and additional data on the space environment during times of anomalous satellite component activity, the authors used the NOAA National Geophysical Data Center to obtain GOES Space Environment Monitor (SEM) data. This sensor suite has provided continuous magnetometer, particle and X-ray data since the mid-1970s, and is a primary source for public, military and commercial space weather warnings[15].

At any point between 1996 and 2012 at least two of the GOES 8 – GOES 15 satellites were collecting data. During this time, several of the GOES satellites were either decommissioned into a parking orbit or experienced technological difficulties and are thus not included in this study. Nonetheless, of the remaining GOES satellites, GOES 12 is the primary satellite used for gathering SEM data, GOES 8, 10, 13 and GOES 14 were also used when one of these satellites was located closer to the anomalous satellite and for dates outside of the and GOES 12 coverage time span.

The SEM consists of three magnetometers, an X-ray/extreme ultraviolet sensor (XRS/EUV), and an energetic particle sensor/high-energy proton and alpha detector (EPS/HEPAD). This study focuses on telemetry from the EPS/HEPAD, which measures the aforementioned particle flux throughout the magnetosphere. Specifically, the instrument consists of two energetic proton, electron and alpha detectors (EPEADs), a magnetospheric proton detector (MAGPD), a magnetospheric electron detector (MAGED), and a high-energy proton and alpha detector (HEPAD)[16].

For this research, the GOES EPS 2 MeV electron flux channel in five-second intervals data is used to assess relativistic electrons at the time of SSPA anomalies. Additionally, the GOES EPS P4 proton flux channel, which measures protons between 15-40 MeV, is used to quantify the high-energy proton flux during the time of each anomaly[15].

C. ACE Data

The ACE satellite has provided operational data since January 1998, and has served as a dominant source for geomagnetic storm warnings. ACE is stationed at the first Lagrangian point (L1), approximately 1.5 million km from the Earth, and is always observing local dayside. Another beneficial aspect of the ACE satellite's stationary location is that in combination with the solar wind speeds, one can calculate the time at which the solar wind carrying energetic particles should contact Earth[16]. The ACE Real-Time Solar Wind System (RTSW) consists of four instruments: Energetic Ion and Electrons (EPAM), Magnetic Field Vectors (MAG), High Energy Particle Fluxes (SIS), and Solar Wind Ions (SWEPAM).

For this study, we use the ACE Satellite's Solar Wind Electron, Proton, and Alpha Monitor (SWEPAM) sensor to quantify Level 2, or verified, solar wind speeds at the time of each SSPA anomaly. This parameter not only characterizes the solar activity during the time of the anomaly, but also provides insight into the respective magnetopause compression. If the solar wind speeds are high (600-800 km/s) then the magnetopause is likely to compress, placing Inmarsat's geostationary communication satellites outside of the magnetosphere where they are unshielded from the harsh space weather environment[17].

D. World Data Center for Geomagnetism in Kyoto

The Geomagnetic Equatorial Dst Data Service is hosted by the World Data Center for Geomagnetism in Kyoto, Japan. The Data Analysis Center for Geomagnetism and Space Magnetism is a part of the World Data Center for Geomagnetism and consists of the Data Center and the University of Kyoto's Graduate School of Science. Several types of geomagnetic indices are calculated at the center that are then verified and archived for public access (e.g. Dst and Auroral Electrojet, AE). Additional parameters, such as Kp and Ap, are derived and also accessible from Kyoto[18].

We used this database for acquiring values of Dst and Kp at times of anomalous satellite component behavior and also to determine dates for severe geomagnetic space weather events between 1996 and 2012.

E. SPENVIS

The Space Environment Information System (SPENVIS), is the European Space Agency's (ESA) primary tool for modeling the effect of the space environment. The figure below was produced using SPENVIS and the NASA's AE-8 Radiation Model embedded in the tool's radiation sources and effects package. AE-8 models the trapped electron flux for a given orbit or location; for this study geosynchronous orbit was selected. This model is the most commonly used radiation model and for high-energy particles, which cause deep dielectric charging, but is not used for fluxes in the few keV range that are responsible

for surface charging[8]. The locations of Inmarsat's satellites are also shown in Figure **3**. It is clear that all geosynchronous satellites, not just those in Inmarsat's fleet, are subject to high electron radiation[19].

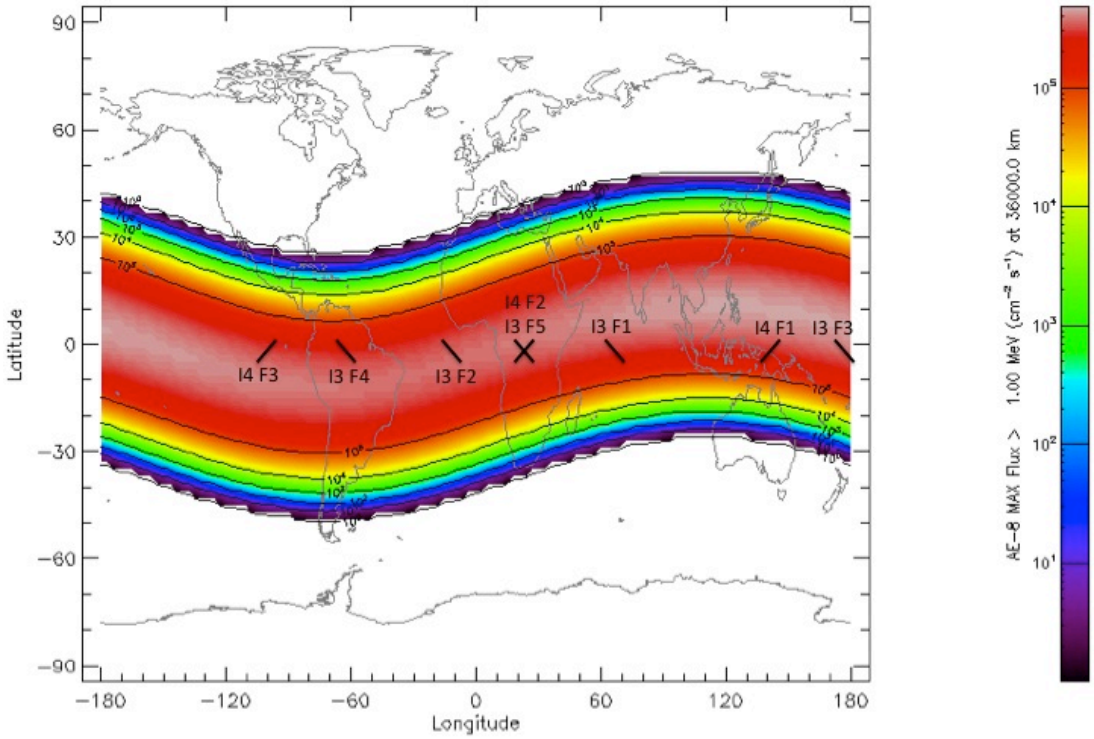

Figure 3: SPENVIS AE-8 Radiation Model with several Inmarsat locations noted.

V. Results and Discussion

A. Telemetry

In this work, we analyzed over 500 MB of SSPA and solar panel telemetry for two generations of Inmarsat satellites. These two fleets have experienced twenty-six SSPA anomalies combined. We concentrate on understanding the space environment at the time of these anomalies. For the SEU analysis, we focus on the four satellites with the heaviest traffic loads, and in the future will extend the analysis to all of the satellites.

The following plot displays the number of SSPA anomalies per year for both satellite fleets. More than fifteen years of anomaly data exists for the first satellite fleet, which experienced no SSPA anomalies prior to the year 2000, and approximately seven years of anomaly data exists for the second fleet. For the first fleet, it is observed that the majority of the anomalies occurred between the years 2000 and 2005. The second fleet experienced anomalies soon after launch. It is possible that these anomalies could be due to space weather, or to differences between the SSPA components and configurations in the two satellite fleets.

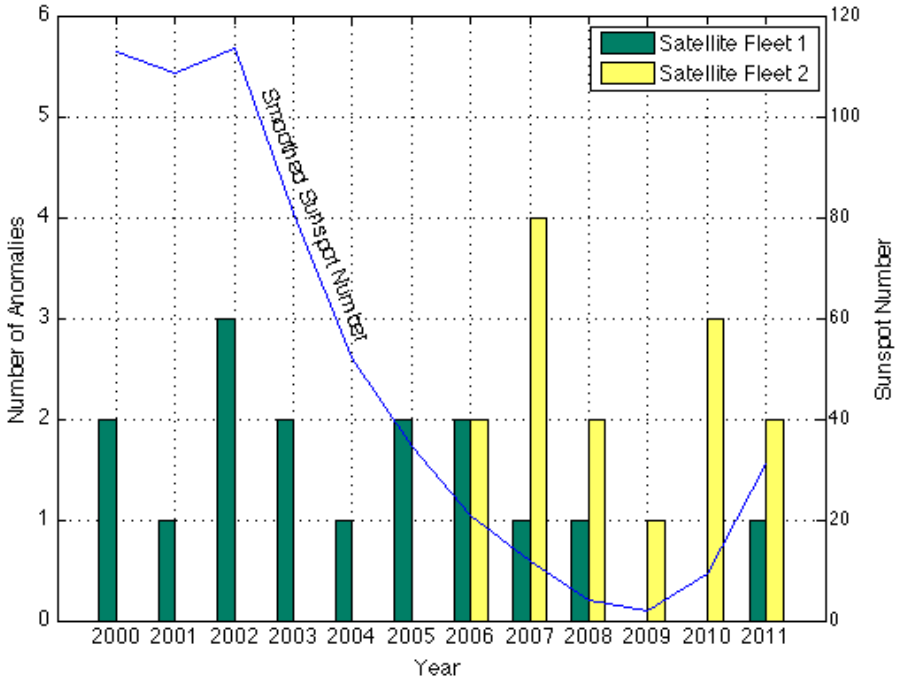

Figure 4: Annual Fleet SSPA Anomaly Totals

Another interesting comparison is between the number of anomalies per year and the solar cycle (designated in Figure **4** by a blue trend-line). The solar maximum for Cycle 23 occurred between 1998 and 2002, and the solar minimum occurred between 2005 and 2008[7]. It is important to note that not all satellite anomalies occur during solar maximum, but that anomalies can occur during solar minimum as well. Since there are likely other factors to consider in addition to solar activity (such as "burn-in" for new satellites and orbital repositioning) we cannot yet draw conclusions whether the anomalies are occurring because of solar maximum or minimum. That said, the year with the most anomalies coincided with the solar minimum of Solar Cycle 23.

Figure **5** shows the age, or number of years after launch, of the satellites when an SSPA anomaly occurred. The age has been approximated to the closest whole year, so 4.6 years is recorded as 5 years. For the second satellite fleet, most anomalies are shown to occur in the first two years of operation. Anomalies that occur during the first two years of a satellite's life are sometimes due to the extreme conditions that the sensors experience during launch and during the maneuvers to reach the allocated orbital slot. However, it is possible that these anomalies are not "burn-in" or transition effects but could be due to harsh space weather events. Of the seven anomalies that occurred during the first two years after a launch, six occurred within two weeks of a severe radiation space weather event caused from relativistic electrons.

Inmarsat satellites have an expected lifetime of fifteen years. One can expect that as the satellite increases in age the likelihood of anomalies should also increase. Nonetheless, there is not an obvious increase in Figure 5 because the two co-plotted fleets consist of satellites at different points in their expected lifetime. While the satellites in the first fleet are up to fifteen years old, the satellites in the second fleet are at most six years old, so the plot is not balanced.

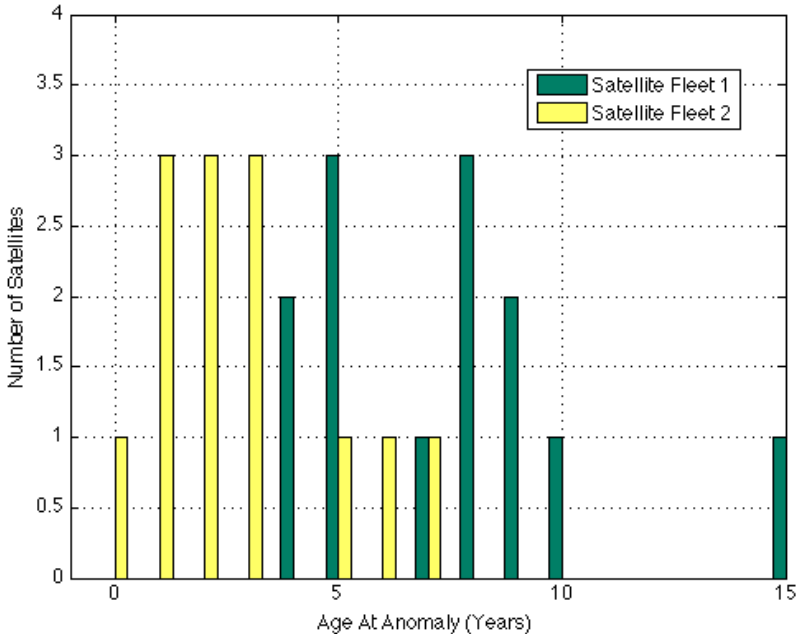

Figure 5: Satellite Age at Time of SSPA Anomaly

Nominal SSPA currents over the lifetime of each satellite have inherent periodicities as a result of traffic, or customers using Inmarsat's communication services. Figure 6 is the single amplitude spectrum for a nominal SSPA. As depicted, the most prevalent periodicities are one week, one day, a half of a day, a third of a day and a quarter of a day.

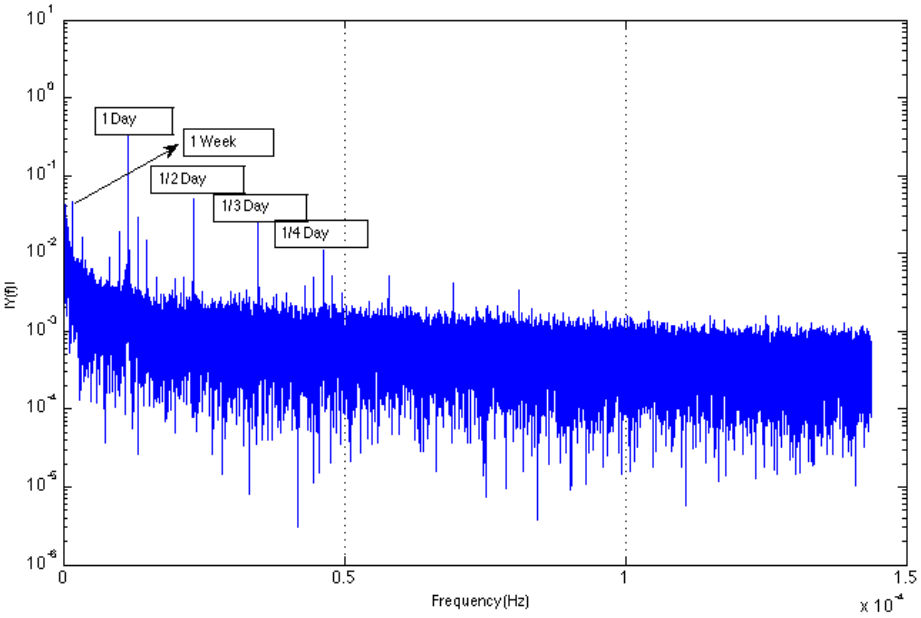

Figure 6: Single Amplitude Spectrum of Nominal SSPA

We observed some cases where the frequency spectrum of an anomalous SSPA showed periodicities in addition to those shown for a nominal SSPA in Figure **6**. In the nominal case, we expect periodicities to be related to traffic and the diurnal cycle. Figure **7** shows an example of the single amplitude spectrum of an anomalous SSPA, where periodicities of 1 day, 1 week, half of a day, one third of a day and a fourth of a day are clearly present, in addition to higher power clusters of harmonics.

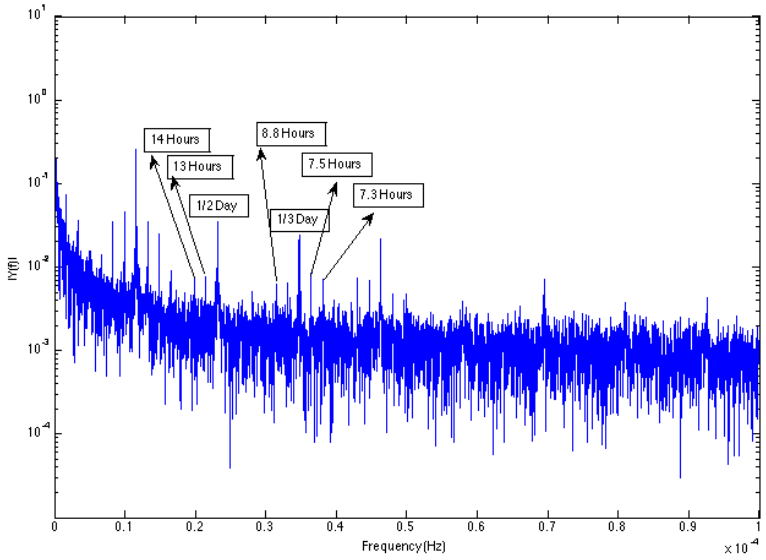

Figure 7: Single Amplitude Spectrum of Anomalous SSPA

B. The Effects of the Space Weather Environment on Satellite Hardware

Relativistic electrons cause bulk charging, and can ultimately lead to circuitry burn out or major satellite anomalies. Bulk charging, or deep-dielectric charging, typically occurs hours to days after large geomagnetic storms, and are the result of high-energy electrons in Earth's VanAllen radiation belts. To quantify the high-energy electrons during the time of each SSPA anomaly, the authors obtained GOES 2 MeV electron flux data for a period of five days prior to each anomaly and one day after. The electron flux data is taken from the GOES satellite that is longitudinally closest to the respective Inmarsat satellite. There are situations when the GOES satellite is located more than fifty degrees away from the Inmarsat satellite. Given the low time resolution of the current study, that should not be a factor in correlation of events with SSPA anomalies.

Figure **8** shows the 2 MeV electron flux (solid blue line) and the SSPA current (dotted green line) five days prior and one day after an SSPA anomaly; the anomaly is designated with a red line.

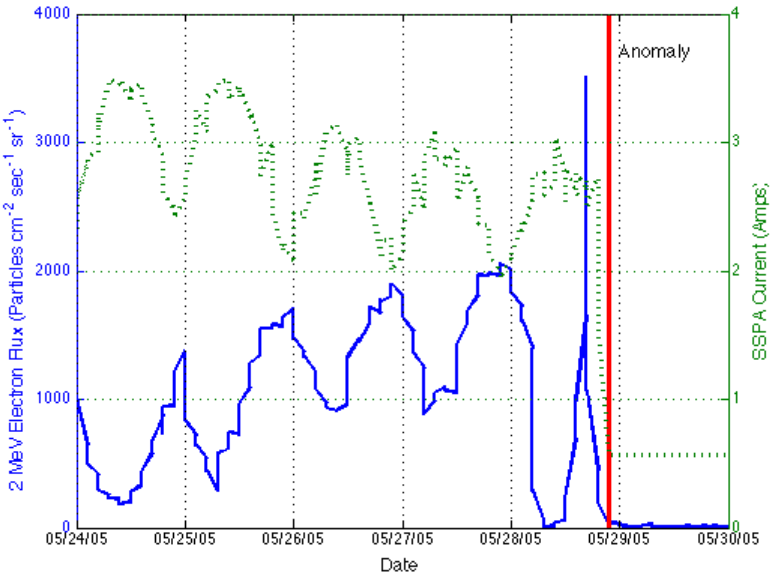

Figure 8: 2 MeV Electron Flux during SSPA Anomaly for five days prior to and one day after an anomaly plotted on the left vertical axis, and SSPA current plotted on the right axis. The GOES 2 MeV electron flux is the blue line, the SSPA current is the dotted green line, and the anomaly is marked with a red line.

The 2 MeV electron flux, shown in the blue solid line, experiences cycles of elevated electron flux until less than 12 hours prior to the anomaly, when the electron flux peaks to approximately 3500 pfu. Immediately following this peak, the SSPA experiences an anomaly. This anomaly is also observed in the SSPA current, plotted in a green dashed line. Interestingly, the SSPA current appears to mirror the trend of the 2 MeV electron flux.

To understand the level of strength of the relativistic electrons at the time of anomaly, the authors examined the 2 MeV electron flux at the time of each of the twenty-six SSPA anomalies. Figure **9** contains the 2 MeV electron flux five days prior and one day after each of the twenty-six SSPA anomalies. The value of the 2 MeV electron flux at failure is designated with a black square.

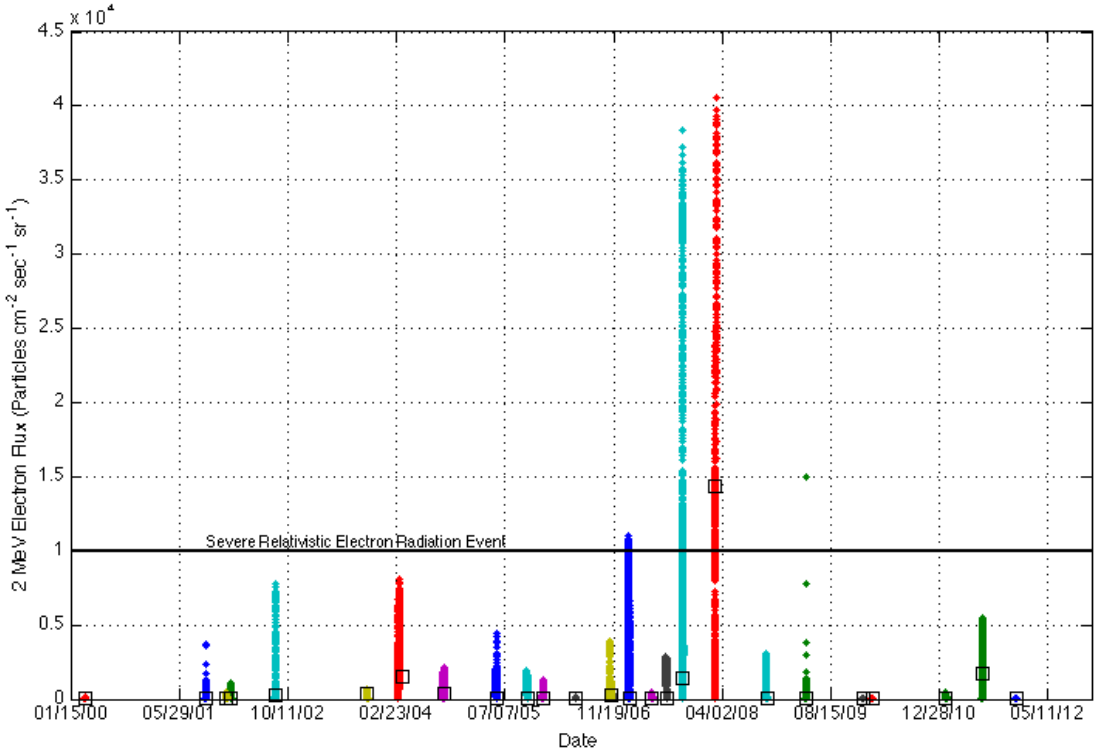

Figure 9: 2 MeV electron flux five days prior and one day after each of the SSPA anomalies, and the 2 MeV electron flux at the time of each SSPA anomaly (black squares).

Out of the 26 anomalies plotted in Figure 9, one anomaly occurred during severe radiation storm conditions (2 MeV electron flux > 10,000 pfu). The remaining SSPA anomalies occurred at times of lower 2 MeV electron flux, with the exception of four SSPA anomalies that occurred when the 2 MeV electron flux was 1440 pfu, 1510 pfu, 1716 pfu, and 4900 pfu. These four SSPA anomalies, and the anomaly that occurred in a severe radiation storm of relativistic electrons are the SSPAs with the five highest amplitudes of electron flux in Figure **9**. These five scenarios of higher 2 MeV electron flux near an SSPA anomaly are also shown in Figure **10** in more detail.

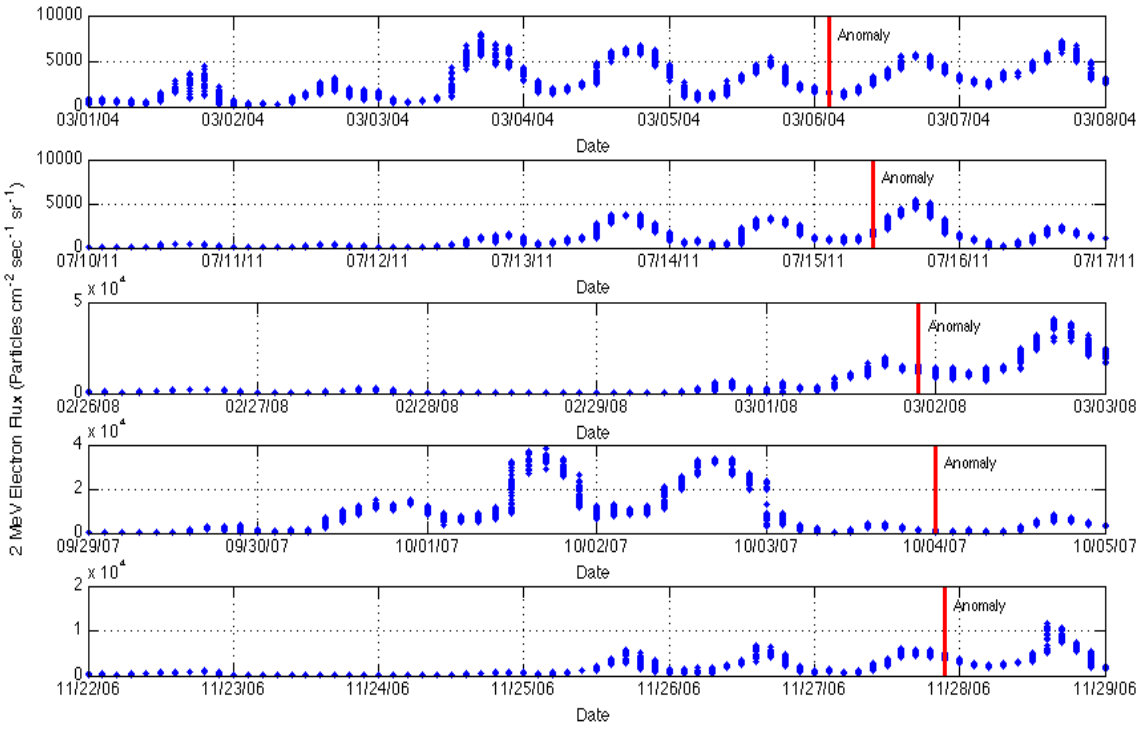

Figure 10: The Five Atypical Scenarios of 2 MeV Electron Flux

All five subplots experience cycles of elevated electron flux, however a distinct pattern does not occur immediately before or after each anomaly. It is important to note that the y-axes are different scales, ranging from 10,000 pfu (the definition of a severe relativistic electron event) and 50,000 pfu. Two instances where the electron flux reaches severe event levels prior to the SSPA anomaly are shown in Figure 10 (c), which occurs less than one day before the anomaly, and 10 (d), which occurs less than two days before the anomaly. The topmost subplot, Figure 10 (a), as well as Figure 10 (b) do not experience severe relativistic electron levels. The bottommost subplot, Figure 10 (e) does not reach severe event levels until less than one day after the anomaly.

In addition to relativistic electrons, high-energy protons can also cause satellite anomalies. While high-energy protons are not well understood, it is believed that these particles are the main cause of hardware anomalies, SEUs and solar array degradation. Similar to the relativistic electrons, the high-energy proton flux during each SSPA anomaly was examined using the GOES 30 MeV proton flux data five days prior and one day after each anomaly. Figure **11** shows the high-energy proton environment during one of the twenty-six SSPA anomalies. The 30 MeV proton flux is shown with a solid blue line, the SSPA current appears as dotted green, and the anomaly is marked with a vertical red line.

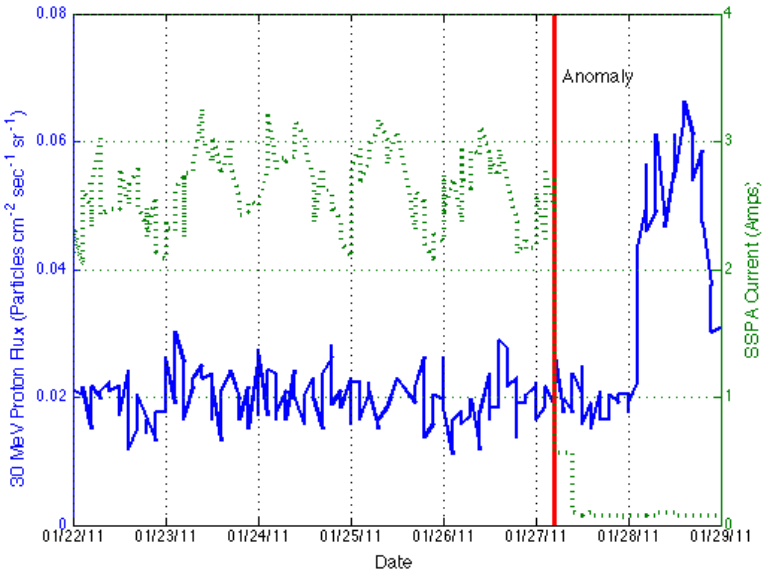

Figure 11: 30 MeV Proton Flux during SSPA Anomaly

The 30 MeV proton flux undergoes slight fluctuations before, during and shortly after the SSPA anomaly, until it experiences a significant increase one day after the anomaly occurs. Unlike the 2 MeV electron flux, the SSPA current does not mirror the proton flux.

Figure 12 contains the 30 MeV proton flux five days prior and one day after each SSPA anomaly, with the 30 MeV proton flux at the time of the anomaly designated with a black square. It is observed that twenty-three SSPA anomalies occur when the 30 MeV proton flux is less than .035 pfu. The three other SSPA anomalies occur when the 30 MeV proton flux is approximately 0.251 pfu, 0.257 pfu, and 0.957 pfu. The SSPA anomaly that occurred on September 29, 2001 with a proton flux of approximately 0.957 is not included in Figure **12** because in the period of five days prior and one day after the SSPA anomaly, the 30 MeV proton flux reached a level of nearly 350 pfu, and thus is a drastic outlier. Additionally, immediately before the five-day period prior to the anomaly, on September 24, one of the six severe space weather radiation storms from SEPs occurred.

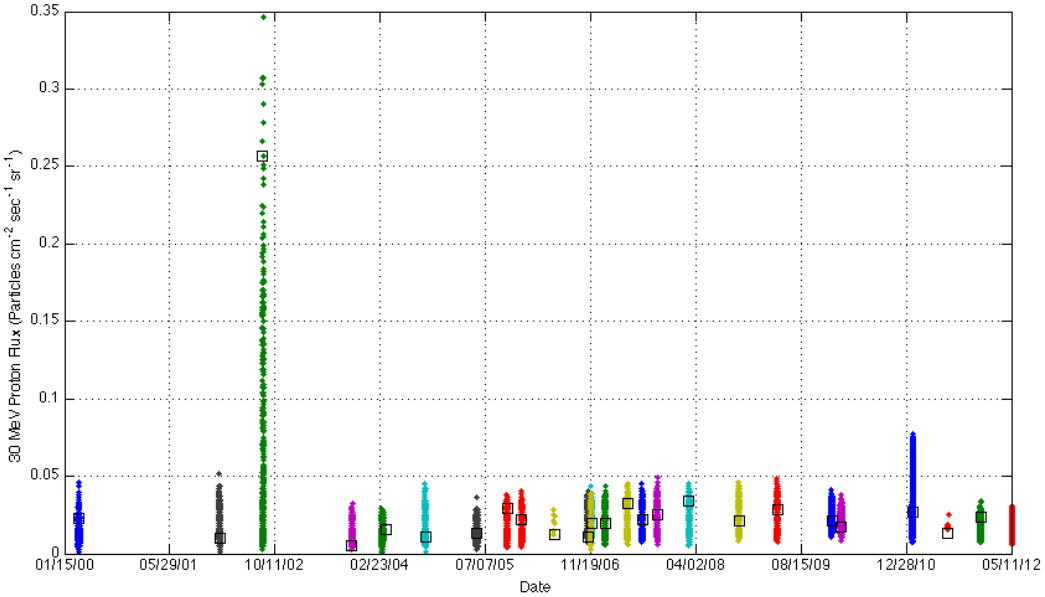

Figure 12: 30 MeV proton flux five days prior and one day after each of the SSPA Anomalies, and the 30 MeV proton flux at the time of each SSPA Anomaly (black squares). The severe SEP radiation event threshold lies at 10,000 pfu and is thus outside of the vertical axis limits.

Twenty-three out of the twenty-six anomalies experience normal levels of 30 MeV proton flux. The three cases of atypical 30 MeV proton flux during the SSPA anomaly are each distinct and are plotted in Figure **13**. The time of the anomaly is designated with a red vertical line.

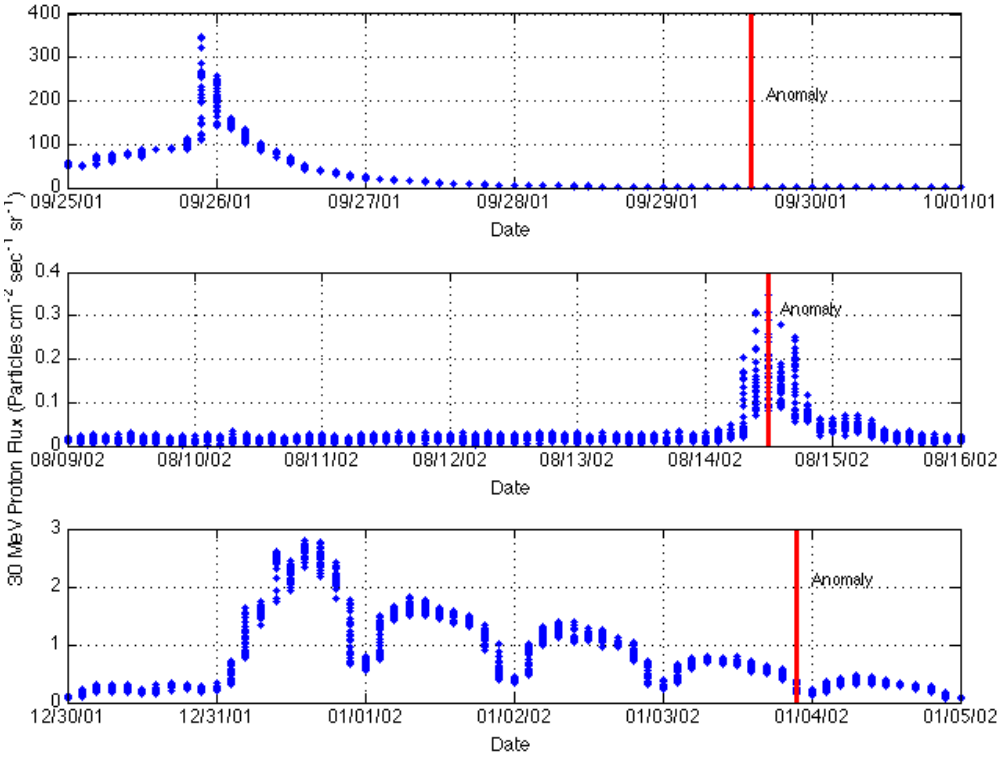

Figure 13: Three SSPA anomalies associated with increased 30 MeV Proton Flux

The topmost subplot of Figure 13 shows elevated levels of 30 MeV proton flux four days before the anomaly occurs. In the period of three days prior and one day after the anomaly the proton flux is observed as nominal. The middle subplot shows nominal 30 MeV proton flux until the day of the anomaly when the proton flux levels increase by a factor of ten. Lastly, the bottommost subplot exhibits a distinctly anomalous trend. Each day before the anomaly there is an elevated and then decreasing pulse of 30 MeV proton flux. The correlation between these three scenarios and the SSPA anomaly is not entirely understood, however there is reason to believe that the elevated levels of 30 MeV proton flux could have contributed to the respective SSPA anomalies. It is unlikely that the proton flux is a major contributor to twenty-three of the twenty-six SSPA anomalies because there is little deviation in the proton flux prior to the anomalies. However, it is possible that the proton flux contributed three of the SSPA anomalies.

Figure **14** consists of three subplots that characterize the geomagnetic space weather environment during the time of SSPA anomaly. Figure **14** (a) is Kp, the general qualitative metric for the geomagnetic field, recorded from Kyoto. Figure **14** (a) shows that the highest Kp value experienced at the time of the 26 SSPA anomalies is Kp = 4. With the Kp scale from 0-9, a level of Kp = 4 is not considered severe geomagnetic space weather conditions. Figure **14** (b) shows Dst also from Kyoto and indicates that at the time of these 26 SSPA anomalies, the geomagnetic field is in a quiet condition.

Lastly, Figure **14** (c) shows the ACE solar wind speed (Vx) and provides insight onto whether the magnetopause is compressed. When the solar wind speed is between 600—800 km/s, the magnetopause may be at risk for compression. When the magnetopause is compressed, satellites located at geostationary orbit are often located outside the protection of the magnetic field and are susceptible to the harsh space weather environment.

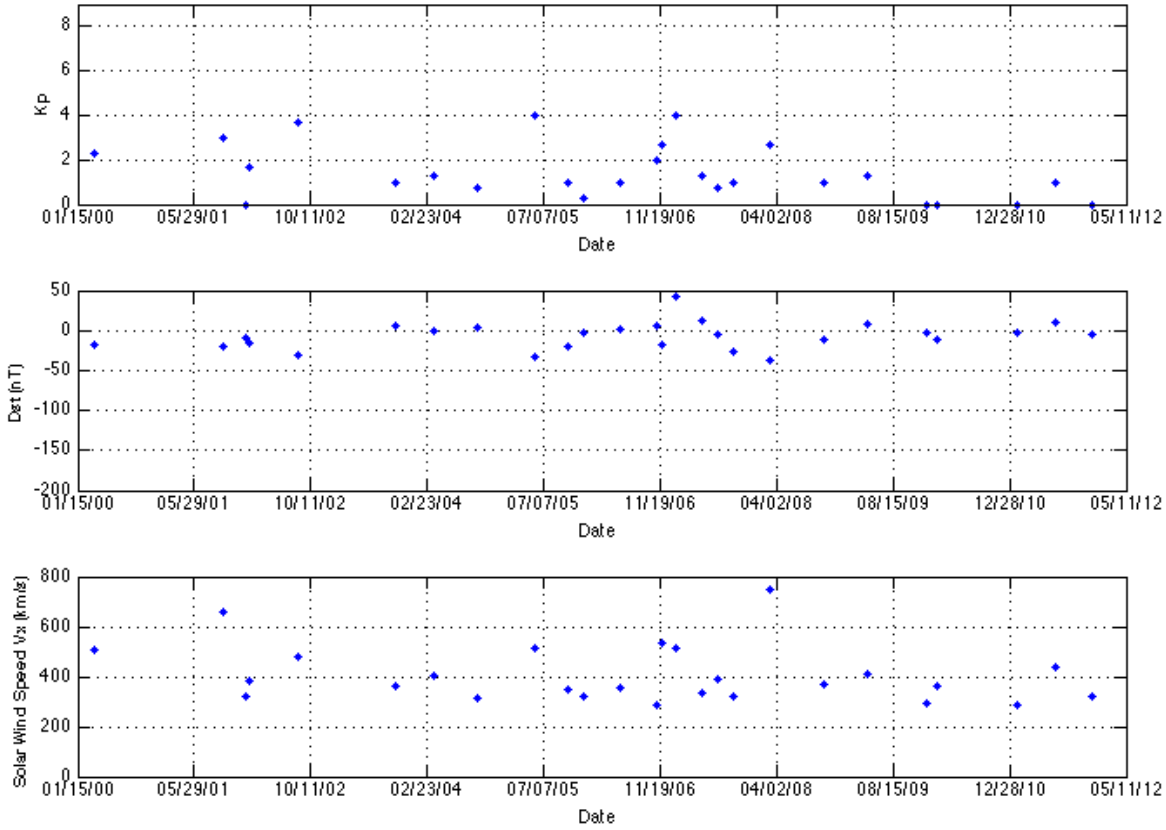

Figure 14: Kp, Dst, and Solar Wind Speed at the time of 26 SSPA Anomalies

Two of the twenty-six SSPA anomalies occurred at times when the magnetopause could have been compressed, or when the satellites could have been located outside of the Earth's magnetic field. Of the two anomalies, one anomaly occurred on September 29, 2001, one of the six most severe space weather radiation events for SEPs, and was the anomaly with the highest 30 MeV proton flux. The other SSPA anomaly that took place when the solar wind could cause magnetopause compression occurred on March 1, 2008, and was the only SSPA anomaly to occur during a severe relativistic electron radiation event. This SSPA anomaly experienced three times the 2 MeV electron flux (14400 pfu) compared to the anomaly with the second highest 2 MeV electron flux (4900 pfu), and experienced more than eight times higher than the SSPA anomaly with the third highest 2 MeV electron flux. Furthermore, the second highest 2 MeV electron flux (4900 pfu) occurred when the solar wind speed was 533.99 km/s, which was highest value apart from the two instances where the solar wind speed was between 600-800 km/s.

VI. Conclusions

In analyzing the correlation between anomalies on seven of Inmarsat GEO communication satellites and space weather phenomena, the authors synthesized eight datasets including four of Inmarsat's historic, archives amounting to more than 500 MB of data (SSPA telemetry, eclipse durations and anomaly/SEUs), and four space weather databases (GOES, ACE, Kyoto and SIDC).

The harsh space weather environment consists of charged particles that can degrade or interrupt electronics on the spacecraft and cause anomalies. Three major types of charged particles are low-energy electrons that can cause surface charging, high-energy electrons that cause bulk charging, and high-energy protons that can cause SEUs and solar array degradation. We have defined severe space weather event as an event that has one of the following: Dst <-200 nT (severe geomagnetic storm), 2 MeV electron flux > 10,000 pfu (severe radiation storm from relativistic electrons), 10 MeV proton flux > 10,000 pfu (severe radiation storm from SEPs), solar flares > Class X10 (severe solar storm).

Out of the twenty-six SSPA anomalies that have occurred in total on the seven Inmarsat satellites, seventeen SSPA anomalies occurred within two weeks of severe space weather events. Fifteen SSPA anomalies occurred during severe relativistic electron radiation events, two SSPA anomalies occurred during severe geomagnetic storms, and one occurred during a severe SEP radiation event as well as a severe relativistic electron radiation event.

It is not conclusive that any of the twenty-six SSPA anomalies were associated with solar minimum or solar maximum, however the year with the most anomalies coincided with solar minimum. Furthermore, no correlation exists between the eclipse seasons and SSPA anomalies or SEUs. This may be due to the additional measures the spacecraft operators take to prepare the satellites for operation during eclipse seasons.

Anomalies that occur in the first two years after launch are generally associated with hazardous launch environments and maneuvers. However, out of seven of the anomalies that occurred during the first two years after launch, six occurred within two weeks of a severe radiation space weather event caused from relativistic electrons.

When analyzing the space weather environment at the time of the anomaly, and specifically the solar wind speed, it was observed that the two instances where the solar wind speed exceeded 600 km/s (likely causing magnetopause compression) were the two most severe anomalies. One anomaly occurred during one of the six most severe space radiation events caused from SEPs, and the other SSPA anomaly was the only anomaly to occur during a severe relativistic electron radiation event.

Preliminary analysis of SSPA current periodicities helps to provide context on the dynamic traffic handled by the SSPAs. Further work is needed to determine the utility of this metric.

It should be noted that anomalies with on-board components, such as SSPAs, are expected and are managed by all satellite operators. Anomaly rates are factored into the design of geostationary satellites and are typically mitigated through the use of on-board unit redundancy and configuration options. The current SSPA anomaly rate presented is significantly lower than that modeled as part of the design reliability analysis; hence both satellite performance and lifetime have not been impacted adversely.

While several correlations between Inmarsat's GEO communication satellites and the space weather environment were observed, future research remains to be completed. The authors plan to gather Los Alamos National Lab (LANL) Magnetospheric Plasma Analyzer (MPA) data to assess low energy electrons that are suspected to induce surface charging. The authors will also work to characterize the space weather environment during the SSPA anomaly for a period greater than five days prior and one day after each anomaly. Additional work comparing the SSPA anomalies, solar wind speed and other space weather parameters to local time will also be conducted.

Furthermore, the authors will complete a more thorough examination of Inmarsat's telemetry for SSPAs and solar arrays for trends that could be used to predict future anomalies from occurring, and will investigate the correlation between solar panel degradation and the space weather environment. We also plan to expand our analysis to include other component telemetry items in addition to those discussed in this work. In addition, we plan to assess the methods for spacecraft shielding and determine whether additional measures for shielding or protection are necessary to increase satellite longevity and performance.

VII. Appendix

Appendix A. Severe Solar Space Weather Event Dates (Solar Flare > X10)

Day	Year	Solar Flare
2-Apr	2001	X14
15-Apr	2001	X17
28-Oct	2003	X17
29-Oct	2003	X10
4-Nov	2003	X18
7-Sep	2005	X17.1

Appendix B. Severe SEP Radiation Event Dates (30 MeV Proton Flux > 10,000 pfu)

Date	Year	Proton Flux (pfu)
14-Jul	2000	24000
8-Nov	2000	14800
24-Sep	2001	12900
4-Nov	2001	31700
22-Nov	2001	18900
28-Oct	2003	29500

Appendix C. Severe Geomagnetic Event Dates (Dst < - 200 nT)

Date	Year	Level (nT)
4-May	1998	-205
25-Sep	1998	-207
22-Oct	1999	-237
6-Apr	2000	-287
7-Apr	2000	-288
15-Jul	2000	-289
16-Jul	2000	-301
12-Aug	2000	-235
17-Sep	2000	-201
31-Mar	2001	-387
1-Apr	2001	-228
11-Apr	2001	-271
12-Apr	2001	-236
6-Nov	2001	-292
24-Nov	2001	-221
29-Oct	2003	-350
30-Oct	2003	-383
31-Oct	2003	-307
20-Nov	2003	-422
21-Nov	2003	-309
8-Nov	2004	-368
9-Nov	2004	-214
10-Nov	2004	-263
15-May	2005	-247

VIII. Acknowledgments

The authors would like to acknowledge Janet Greene, Mark Dickinson, Marcus Vilaca, Cathryn Mitchell, Joe Kinrade, the Invert Centre for Imaging Science at the University of Bath, Greg Ginet, Trey Cade, Dr. Fred DeJarnette, the Inmarsat Spacecraft Analysts, and Joseph Ditommaso for their support. The authors would also like to thank NOAA, LANL, ACE, SIDC and the World Data Center for Geomagnetism for access to their space environment databases. Additionally, the authors would like to thank NSF, MIT, and Inmarsat for funding this work.

IX. References

[1]Baker, D.N. “The Occurrence of Operational Anomalies in Spacecraft and Their Relationship to Space Weather” *IEEE Transactions on Plasma Science* 28.6 (2000): 2007-2016.

[2]Wilkinson, D.C., Shea, M.A., Smart, D.F. “A Case History of Solar and Galactic Space Weather Effects on the GEO COMSAT TDRS-1”.

[3]Gubby, Robin, and John Evans. "Space Environment Effects and Satellite Design." *Journal of Atmospheric and Solar-Terrestrial Physics* 64.16 (2002): 1723-733.

[4]Baker, D. "What Is Space Weather?" *Advances in Space Research* 22.1 (1998): 7-16.

[5]Baker, Daniel N. "How to Cope with Space Weather." *Science* 297 (2002): 1486-487. Print.

[6]Cole, David G., “Space Weather: Its effects and predictability” *Space Science Reviews* 107 (2003): 295-302.

[7]Royal Observatory of Belgium. "SIDC - Solar Influences Data Analysis Center." *SIDC - Solar Influences Data Analysis Center*. 28 Aug. 2003. Web. 25 June 2012. <http://sidc.oma.be/sunspot-data/>.

[8]Vampola, A. L. *The Aerospace Spacecraft Charging Document*. [S.l.]: Space Division, Air Force Systems Command, 1985. Print.

[9]Lanzerotti, “Space Weather Effects on Communications” *NATO Science Series: Space Storms and Space Weather Hazards* 38 (2001): 313-334.

[10]Baker, D.N. “Effects of Hostile Space Weather on Satellite Operations,” *IEEE International Symposium on Electromagnetic Compatibility (EMC)*. 14-19 Aug. 2011. 306-311.

[11]Thomsen, M. F., M. H. Denton, B. Lavraud, and M. Bodeau. "Statistics of Plasma Fluxes at Geosynchronous Orbit over More than a Full Solar Cycle." *Space Weather* 5.3 (2007): 1-9.

[12]Balch, Christopher. "The K-Index." *Space Weather Prediction Center*. NOAA National Geophysical Data Center, 12 Dec. 2011. Web. 20 Feb. 2012. <http://www.swpc.noaa.gov/info/Kindex.html>.

[13]Mursula, “A New reconstruction of the Dst index for 1932 – 2002” *Annales Geophysicae* 23:2 (2005): 475-485.

[14]National Weather Service. "NOAA / NWS Space Weather Prediction Center." *NOAA / NWS Space Weather Prediction Center*. National Oceanic and Atmospheric Administration, 5 Nov. 2007. Web. 23 Mar. 2012. <http://www.swpc.noaa.gov/>

[15]*GOES I-M Databook.* Palo Alto, CA: Space Systems/Loral, 1996. Print.

[16]The National Space Weather Program Council. "National Space Weather Implementation Plan, 2nd Edition." *The National Space Weather Program*. Office of the Federal Coordinator for Meteorology, July 2000. Web. 17 July 2012. <http://www.ofcm.gov/nswp-ip/tableofcontents.htm>.

[17]ACE Science Center. "New ACE Level 2 Data Server." *ACE Level 2 Data Server*. NASA, 21 Apr. 2008. Web. 1 May 2012. <http://www.srl.caltech.edu/ACE/ASC/level2/new/intro.html>.

[18]World Data Center for Geomagnetism, Kyoto. "Geomagnetic Equatorial Dst Index Home Page." *Geomagnetic Equatorial Dst Index Home Page*. Data Analysis Center for Geomagnetism and Space Magnetism, n.d. Web. January 2012. <http://wdc.kugi.kyoto-u.ac.jp/dstdir/index.html>.

[19]European Space Agency. "SPENVIS - Space Environment, Effects, and Education System." *SPENVIS - Space Environment, Effects, and Education System*. ESA, 1997. Web. 1 March 2012. <http://www.spenvis.oma.be/intro.php>.